



Characteristic and adsorption properties of zirconia aerogel and xerogel nanostructure application to fluoride removal from drinking water of Tunisian south region

Nesrine Kamoun^{a,b,*}, Soumaya Mezghich^c, Lamjed Mansour^d, Mohamed Kadri Younes^b, Hamza Elfil^a

^aUniversity of Carthage, Desalination and Natural Water Valorization Laboratory, Center of Water Research and Technologies, Ecopark of Borj-Cedria, BP 273 Soliman 8020, Tunisia, emails: nesrinekamoun22@gmail.com (N. Kamoun), elfilhamza@gmail.com (H. Elfil)

^bLaboratory of Chemistry of Materials and Catalysis, Department of Chemistry, Faculty of Sciences of Tunis, University Tunis El Manar, 2092 Tunis, Tunisia, email: mohameddyounes12@gmail.com (M.K. Younes)

^cUniversité Clermont Auvergne, Institut de Chimie de Clermont-Ferrand (ICCF), CNRS, BP 10448, F-63000 Clermont-Ferrand, France, email: soumaya.mezguich@gmail.com (S. Mezghich)

^dZoology Department, College of Science, King Saud University, Riyadh, Saudi Arabia, email: lmansour@ksu.edu.sa (L. Mansour)

Received 20 March 2022; Accepted 10 July 2022

ABSTRACT

The present investigation reports the effect of the solvent evacuation mode in the preparation step of zirconia adsorbent, in removal adsorption fluoride from tap water in southern Tunisia. Aerogels and xerogels zirconia were prepared in one-step by the sol-gel method. Aerogels are obtained by drying under supercritical conditions of solvent while xerogel are obtained by ordinary drying in an oven. The characteristic properties of those solids were investigated using Fourier transform infrared spectroscopy (FTIR), X-ray diffraction (XRD), Rietveld refinement of XRD patterns, N₂ physisorption (BET), scanning electron microscopy, transmission electron microscopy and energy-dispersive X-ray spectroscopy. Experimental parameters such as adsorbent dose, contact time, initial fluoride concentration and pH value were investigated. Crystallite size showed by Rietveld refinement indicated that all crystalline xerogel and aerogel zirconia samples were of nano-crystalline nature with crystallite size in the range of 16–18 nm. Textural analysis, carried out by BET, reveals that all adsorbents are characterized by a developed mesoporous texture, high surface area and large porosity. FTIR spectra spectroscopy shows the important role of superficial hydroxyl groups in the defluorination process. The different obtained results confirmed that the efficiency of xerogel zirconia for the fluoride elimination is better than that of aerogel zirconia. The selected xerogel zirconia presents a high fluoride removal rate of about 100% in the wide pH range (2–7) with a low adsorbent dose (30 mg) and a lower equilibrium time of 25 min. Xerogel zirconia successfully reduce fluoride from natural water with a concentration of 3.83 mg L⁻¹, to a value lower than the standard Tunisian set at 0.8 mg L⁻¹, even in complex matrix.

Keywords: Fluoride adsorption; Zirconia; Mesoporous; Xerogel; Aerogel; Drinking water

* Corresponding author.

1. Introduction

The contamination of surface water and groundwater, which are two important sources of drinking water, by fluorides is a worldwide concern in recent times [1]. In the south of Tunisia, especially in the regions of Gafsa, Métaoui, Medenine, Tataouine and Redayef, fluoride contents in drinking water can reach 3 mg L^{-1} [2]. Fluoride is needed for human health, but it becomes toxic and causes dental and skeletal fluorosis [3] once its concentration exceeds the maximum concentration levels of fluoride of 1.5 mg L^{-1} , recommended by WHO, in drinking water [4].

Many technologies have been applied for defluoridation of drinking water, including membrane processes [5], chemical precipitation [6], ion exchange and adsorption [7,8]. Among these methods, adsorption is the most economic and efficient methods to provide safe drinking water [9]. Different adsorbents for fluoride removal have also been developed, such as activated alumina [10], silica gel [11], zeolites [12], metal oxides [13], activated carbon, and resins [7].

Recently, a new class of fluoride adsorbent based on metal oxide attracts great attention specially zirconia, which is a very interesting material because of its thermal stability, mechanical resistance, and excellent removal capacity of toxic pollutants. It is considered as a potential fluoride adsorbent due to its high electrical affinity for fluoride [14]. It is well known that the adsorption ability depends on the physico-chemical properties of materials which are highly influenced by the preparation method [15]. Recently, gels are considered as the efficient materials for removal pollutants [16]. The sol-gel process seems to be an attractive route for the synthesis of these oxides using one step. In fact, compared to the conventional methods, the sol-gel method provides the ability to control the structure and composition of the final solid mix at a molecular level [17]. This method, offers a good homogeneity of the different precursors [18]. One of the important steps in the sol-gel method is solvent elimination after gelation [19]. This step seems to affect textural, structural, active site stability and removal capacity of adsorbent.

In the same context, the main objective of the present study was to investigate the effect of some preparation conditions such as drying mode and calcination temperature on capacity of zirconia materials in the defluoridation of water. For this purpose, we are interested to prepare mesoporous xerogel and aerogel zirconia at various calcination temperature and to determine the best conditions of both heat process and drying mode for water defluoridation optimization.

Most advantageous parameters for water defluoridation such as contact time, adsorbent dose, initial fluoride concentration and pH adsorbent value were carried out. Selected adsorbent was tested on natural contaminated water. To our knowledge, this work is the first attempt for studying the effect of solvent evacuation conditions on adsorbent properties of zirconia solid for fluoride removal.

2. Experimental section

2.1. Adsorbent preparation

Zirconium butoxide $\text{Zr}(\text{O}i\text{Bu})_4$ (Aldrich 80% in 1-butanol) is first of all dissolved in 1-butanol followed by acid nitric

addition with a 0.5 molar ratio ($n_{\text{HNO}_3}/n_{\text{Zr}} = 0.5$). Finally, water was slowly added to obtain gel with hydrolysis ratio $n_{\text{H}_2\text{O}}/n_{\text{Zr}} = 3$.

After gelification, alcogel solution was divided into two parts; afterward dried at different conditions to obtain xerogel and aerogel samples. Xerogel was obtained by drying alcogel solution in an oven ($T = 110^\circ\text{C}$) at atmospheric pressure for 24 h. While aerogel was obtained under supercritical conditions ($T = 289^\circ\text{C}$, $p = 40 \text{ bar}$), by drying the alcogel solution in an autoclave during 3 h. The resulting solid was calcined under a flow of oxygen at 500°C with a heating rate of 3 K min^{-1} during 3 h.

The sorbents are named XZ for non-calcined xerogel, XZ-T for calcined xerogel, AZ for non-calcined aerogel and AZ-T for calcined aerogel where T is temperature calcinations. All reports listed ($n_{\text{HNO}_3}/n_{\text{Zr}}$, $n_{\text{H}_2\text{O}}/n_{\text{Zr}}$) are optimized.

2.2. Adsorbent characterization

Textural and structural characterization was performed by a Micromeritics Apparatus (type ASAP 2000), derived from a computer-type AST. Samples were first degassed for 4 h under vacuum at 473 K. Specific surface areas and pore size distributions were determined by BET and Barrett-Joyner-Halenda (BJH) methods, respectively.

X-ray diffraction (XRD) patterns were obtained on an automatic Philips PANalytical diffractometer using $\text{CuK}\alpha$ radiation ($\lambda = 1.5412 \text{ \AA}$) and nickel monochromator. Reticular distances calculated are compared to those given by the Joint Committee on Powder Diffraction Standards. Lattice parameters were refined by the Rietveld method with General Structure Analysis Software (FullProof). Crystallite size of ZrO_2 tetragonal phase was determined from the characteristic peak ($2\theta = 30$) using Scherrer equation $D = K\lambda/\beta\cos\theta$, where $K = 0.9$, D represents the crystallite size, $\lambda = 1.5412 \text{ \AA}$ Cu $\text{K}\alpha$ radiation wavelength and β the corrected half width of the diffraction peak.

Fourier transform infrared spectroscopy (FTIR) spectra of the samples diluted in KBr were recorded with a SHIMADZU, IR Affinity-1 spectrometer over a range of $4,000\text{--}400 \text{ cm}^{-1}$ in the transmission mode.

Material morphological structure before and after fluoride removal were determined using an ultra-high-resolution analytical electron microscope (HR-FESEM Hitachi SU-70).

For transmission electron microscopy (TEM) observations, samples were dispersed in ethanol by applying the ultrasonic wave and were collected on a holly micro-grid supported on a copper grid mesh. An emission field type TEM (JEOL JEM2010F) operated at 200 kV was used for the observations. The chemical compositions of the synthesized samples were confirmed by energy dispersive X-ray spectroscopic analysis (EDAX) using an X-ray detector attached to the TEM instrument.

The pH at the point of zero charge (pHpzc) of the xerogel material was determined by batch equilibration technique. In several flasks, 20 mL of 0.1 M NaCl was taken and initial pH was adjusted from 2 to 10 using dilute HCl and NaOH solutions. To each flask, 50 mg of the xerogel adsorbent was added. The solutions were stirred for

24 h. The solution was then filtered and the final pH was measured.

2.3. Batch adsorption experiments

Defluoridation experiments were performed by mixing the adsorbent with fixed volume (20 mL) of fluoride solution (NaF solution of initial concentration varying from 2 to 10 mg L⁻¹ (batch adsorption technique). All adsorption experiments were carried out using a magnetic Multistirrer VELP scientifica with a stirring speed of 300 rpm. The solution was then filtered by filter paper with 4 μm of porosity. By means of fluoride ion selective electrode (ISE model no. 6.0502.150, Metrohm Switzerland) the fluoride ion concentration, before and after adsorption, was determined. The ion meter was calibrated before every use. The detection limit is 20 μg L⁻¹.

Fluoride percent ions removal was calculated by the following relation:

$$\% \text{ Removal} = \frac{C_o - C_e}{C_o} \times 100 \quad (1)$$

where C_o and C_e are the initial and equilibrium liquid phase concentrations in mg L⁻¹ of ion fluoride.

3. Results and discussion

3.1. Characterization of xerogel and aerogel zirconia adsorbent

X-ray diffraction patterns of calcined xerogel and aerogel solids are given in Fig. 1 and Table 1. Relative content of crystalline phases, crystalline size and lattice parameters were estimated and determined by Rietveld analysis (Table 1).

Dried xerogel solids are seen to be completely amorphous (Fig. 1). This result is in well accordance with Patel et al. [20] studies; interested to Al₂O₃/ZrO₂ solids preparation. The xerogel calcined at 300°C develops a pure tetragonal zirconia phase characterized by peaks at 2θ = 30°, 50° and 60° (JCPDS 17-0923). After calcination at 500°C, the XZ-500 sample still exhibits the tetragonal ZrO₂ phase with a few percentages of monoclinic zirconia phases (2θ at 24°, 28° and 31°). However, calcined aerogels (AZ-300, AZ-500) stabilize tetragonal zirconia phase even at 500°C, suggested supercritical evacuation mode of solvent, playing an important role in the stability of metastable tetragonal zirconia phase. In fact, in the aerogel procedure, no tetragonal-monoclinic phase transition was observed even at high calcinations temperature. The dried aerogel is amorphous.

Furthermore, crystallite size determined from X-ray diffraction data (Table 1) showed that all crystalline zirconia

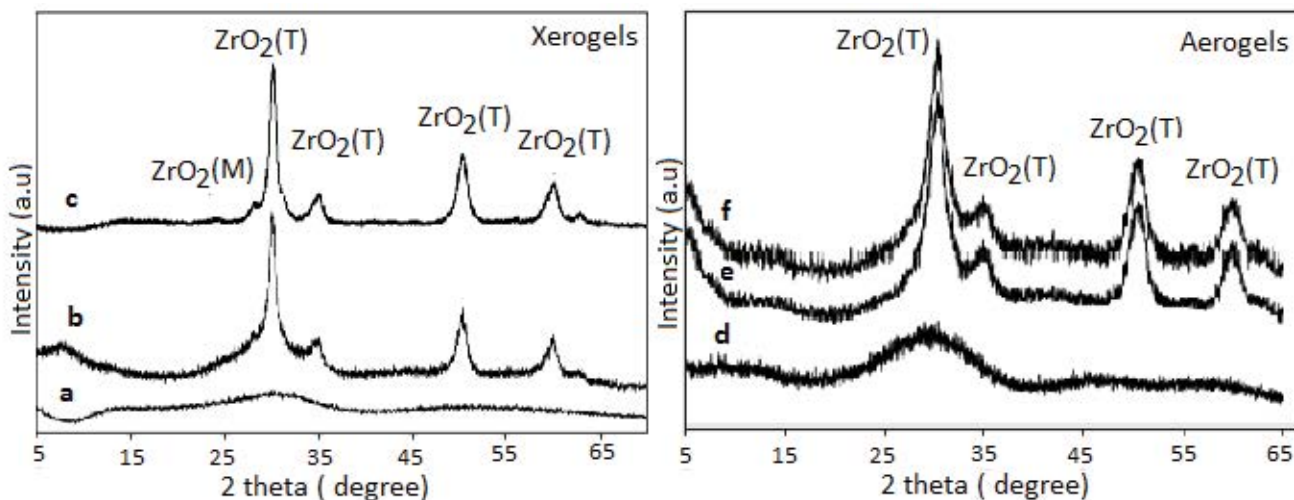


Fig. 1. XRD patterns of xerogels and aerogels non-calcined and calcined at different temperatures: (a) XZ non-calcined, (b) XZ-300, (c) XZ-500, (d) AZ non-calcined, (e) AZ-300 and (f) AZ-500.

Table 1

Crystallite size of solids and structural parameters of the tetragonal and monoclinic zirconia phase

Adsorbents	Crystallite size (nm)	Phase	% of ZrO ₂ phase	Lattice parameters (Å)		
XZ	–	–	–	–	–	–
XZ-500	17.582	Tetragonal	88.46	3.6367	3.6367	5.1838
		Monoclinic	11.54	5.1832	5.1564	5.2821
AZ	–	–	–	–	–	–
AZ-500	18.331	Tetragonal	100	3.6234	3.6554	5.1710

adsorbent were of nano-crystalline nature with crystallite size in the range of 16–18 nm.

Textural characterization was evaluated by means of nitrogen adsorption–desorption isotherms at 77 K. BET isotherms are of type IV (Fig. 2), according to IUPAC classification [21], characteristic of mesoporous materials. It has been reported that mesoporous materials are excellent adsorbents since they provide large surface area compared to macroporous materials and present better access to adsorbate into the pores compared to microporous materials [22]. Nevertheless, the hysteresis loop of adsorbent is of type H3 which corresponds to broad pores resulting from texture in layers [21]. Pore size distribution curve determined by BJH method for all adsorbents are bimodal with pores size centered at 29 and 145 Å for XZr, at 45 and 154 Å for XZr-300 and at 31 and 154 Å for XZr-500, indicating a heterogeneous distribution. Results revealed that adsorbents specific surface areas decrease with temperature calcinations increasing (Table 2).

Specific surface area of XZr ($448 \text{ m}^2 \text{ g}^{-1}$) decrease about 84% after heating at 500°C , due probably to sintering thermal. According to this work and several previous one, the use of sol–gel method in one-step allow to synthesize adsorbent with developed texture [22]. As reported by Wang et al. [23] prepared $\text{CeO}_2\text{-ZrO}_2$ nanocages adsorbent by sol–gel method in one-step can remove 98% fluoride ion from aqueous solution, however the materials exhibit a low surface area ($29.6 \text{ m}^2 \text{ g}^{-1}$). At the same context, Chang et al. [24] have demonstrated that synthesized superpara-magnetic $\text{ZrO}_2/\text{SiO}_2/\text{Fe}_3\text{O}_4$ present a high adsorption properties for fluoride removal yet it develops a low specific surface area compared to our XZr material before calcination.

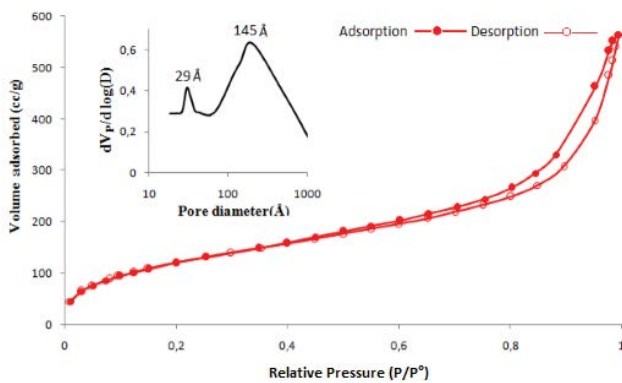


Fig. 2. Adsorption–desorption isotherm and BJH pore distribution of xerogel adsorbent.

Table 2
Textural properties of solids

Adsorbents	S_{BET} ($\text{m}^2 \text{ g}^{-1}$)	V_p ($\text{cm}^3 \text{ g}^{-1}$)	D_p (Å)
XZ	448	0.77	85
XZ-500	68	0.25	123
AZ	533	1.05	98
AZ-500	240	0.30	55
XZ-F	244	0.32	78

It can be concluded that this method permit to synthesized materials with developed high adsorption capacity and a higher developed texture [22].

In another hand, material drying under supercritical conditions confers on solid more developed texture. It can be seen that non-calcined aerogel zirconia AZ shows the highest area ($533 \text{ m}^2 \text{ g}^{-1}$) in comparison with dried xerogel zirconia XZ ($448 \text{ m}^2 \text{ g}^{-1}$). This difference is probably due to evacuation solvent mode. Indeed, when the solvent is removed under atmospheric conditions in an oven, the liquid–vapor interface within the gel is created due to surface tension, which acts on the pores and causes their shrinkage. However, under supercritical conditions, the liquid–vapor interface disappears and therefore no capillary pressure forms during drying. As it appears from Fig. 4, isotherms of aerogels solids are of type IV with H2 loop characteristic of mesoporous materials with uniform channel-like pores [21]. The BJH porous distribution of the aerogels zirconia (Fig. 3) is monomodal and reflect a homogeneity of the porosity. The aerogel specific surface area decrease ($240 \text{ m}^2 \text{ g}^{-1}$) after calcination at 500°C , which related to a sintering phenomenon.

FTIR spectra of all dried and calcined xerogel solids are given in Fig. 4. The region of hydroxyl groups seems also affected by the drying mode as well as by the calcinations temperature.

Xerogel zirconia adsorbent exhibit a wide peak centered at 3468 cm^{-1} attributed to the stretching vibration of hydroxyl group [25] and a fine peak located at 1629 cm^{-1}

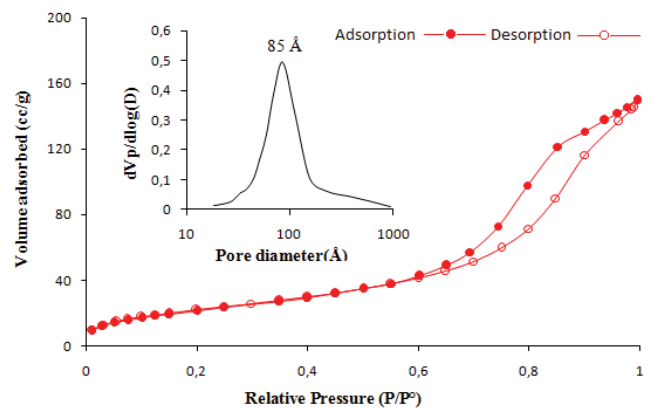


Fig. 3. Adsorption–desorption isotherm and BJH pore distribution of aerogel adsorbent.

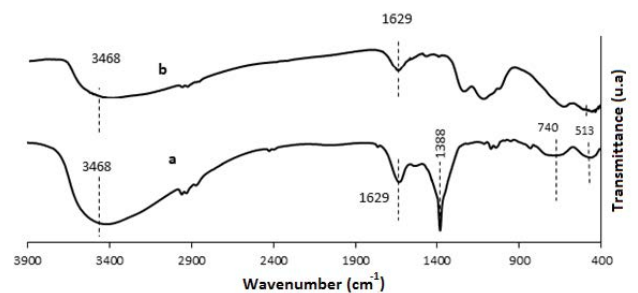


Fig. 4. IR spectra of xerogels: (a) XZ and (b) XZ-500.

characteristic of non-dissociated water molecules (δHOH) [26]. Indeed, we note a band at 1388 cm^{-1} , assigned to bending vibration of Zr-OH functional group [27]. Peaks at 513 and 740 cm^{-1} are characteristic of Zr-O in ZrO_2 [14]. Bands at 2846 and 2943 cm^{-1} correspond to organic residue [28]. Moreover, the peak at 1380 cm^{-1} almost disappeared after calcination at 500°C . Indeed, a significant decrease in the intensities of peaks at 3468 and at 1629 cm^{-1} was observed with heat treatment. This result shows that calcination decrease the number of surface hydroxyl groups which are an active site for adsorption fluoride [20]. In addition, the FTIR spectra of aerogel adsorbents (Fig. 5) show a decrease of intensity bands of hydroxyl group (1616 and 1388 cm^{-1}) and a shift of the band at 3468 cm^{-1} , in comparison with xerogel materials. The band at 1536 cm^{-1} corresponds to Zr-H [29]. Therefore, this result reveals the effect of evacuation mode of solvent on the stability of hydroxyl group, which are more stable in xerogel solid. In addition, after calcinations of aerogel material (Table 3) at 500°C , we note the disappearance of bands of hydroxyl group.

3.2. Optimization of the synthesis parameters

3.2.1. Effect of calcination temperature

Effect of heat treatment of zirconia on fluoride removal is carried out, and results were shown in Fig. 6.

It is well known that the adsorption ability is highly influenced by the heat treatment of metal oxide [30]. Effect of calcination on defluorination capacity of the materials shows that the non-calcined xerogel zirconia exhibits the best removal rate ($\sim 100\%$). This result can be linked to the developed texture of the solid and to the sol-gel method adopted during the preparation materials. It has been reported [15] that the hydrolysis reaction, which occurs between the metal oxide and water, leads to the

formation of hydroxyl groups on the surface of oxides metal, considered to be active adsorption sites for anions in aqueous solution [20]. However, xerogel calcination at 300 and 500°C decreases its adsorption capacity by approximately 13% and 20% for both masses. Maximum amounts of fluoride adsorption by calcined solids at 300°C and 500°C reach 87% and 79% , respectively. This decrease in adsorption ability can be justified by the decrease in the specific surface area of about 80% and by the loss of surface hydroxyl group, during calcination. Many studies has reported that the hydroxyl group played an important role in the adsorption process via the ions exchange and complexation [23,31]. This result is confirmed by infrared spectroscopy (Fig. 4) that indicated a significant decrease in the intensity of the absorbance band of hydroxyl groups and the disappearance of the relative band to Zr-OH groups. Furthermore, this result is also approved by XRD that demonstrates the large loss of surface hydroxyl group, during the heat treatment. This loss is related to the phase transformation from amorphous ZrO_2 to tetragonal ZrO_2 phase, with the dehydroxylation of Zr-OH into ZrO_2 . Similar results are in accordance with others done by Yu et al. [25] and Wang et al. [23].

Non-calcined aerogel zirconia (Fig. 7) shows a greater percentage of fluoride removal than calcined aerogels, which can be explained by the loss of hydroxyl groups with heating treatment. This result can also be attributed to the decrease of the surface area of aerogel adsorbent after heating (Table 2).

3.2.2. Effect of solvent evacuation mode

It was reported that adsorbent properties of materials are highly influenced by textural and structural properties, which are extremely sensitive to drying procedure [28].

The effect of drying mode of zirconia gel on fluoride adsorption was carried out for initial anion fluoride concentrations of 5 mg L^{-1} . Xerogel zirconia presents a high amount of fluoride adsorption in comparison with aerogel zirconia adsorbent (Fig. 8). These results can be related to more active and accessible adsorption sites to interact with fluoride ion in xerogel ZrO_2 adsorbent. These sites are of two pores types in comparison with those of aerogel adsorbent, characterized by the existence of one type of pore. Thus, In the case of xerogel, the simultaneous presence of large specific surface area (more than $200\text{ m}^2\text{ g}^{-1}$) and mesoporous structure with various types of pores expose a large number of available active sites and channels. These effects increase the diffusion efficiency and promote the adsorption performance of fluoride.

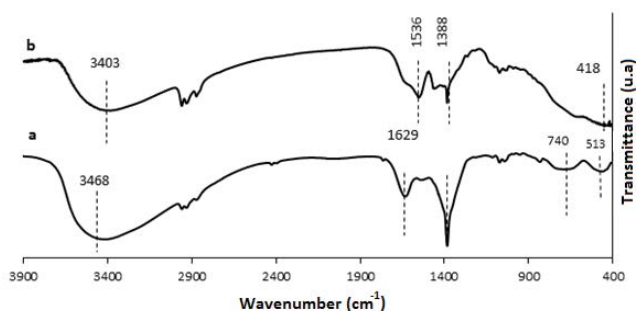


Fig. 5. IR spectra of xerogel and aerogel: (a) XZ and (b) AZ.

Table 3
Attribution of IR bands of different adsorbents

Functional group	Zr-OH	δHOH	Zr-H	Zr-OH	Zr-O
Adsorbents			Frequency (cm^{-1})		
XZ	3468	1629	–	1388	513–740
XZ-500	3468	1629	–	–	513–740
AZ	3403	1629	1536	1388	418
AZ-500	3403	–	1536	–	418

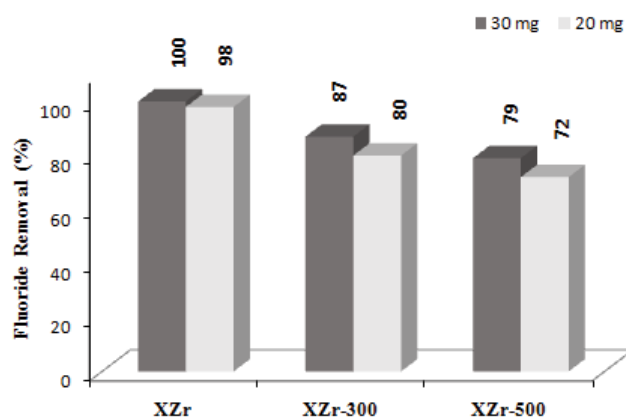


Fig. 6. Effect of calcination temperature of xerogel adsorbent on the fluoride removal ($[F^-] = 5 \text{ mg L}^{-1}$; $\text{pH} = 7$; contact time = 35 min; temperature ($T = 25^\circ\text{C}$)).

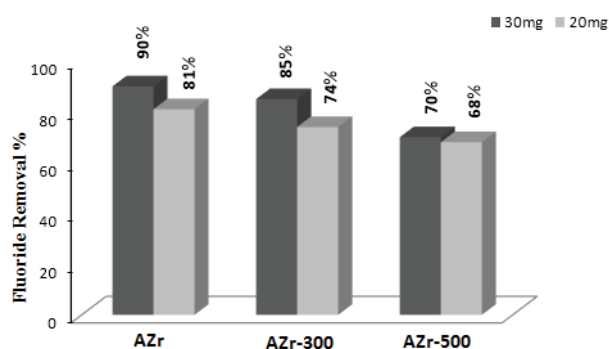


Fig. 7. Effect of calcination temperature of aerogel adsorbent on the fluoride removal ($[F^-] = 5 \text{ mg L}^{-1}$; $\text{pH} = 7$; contact time = 35 min; temperature ($T = 25^\circ\text{C}$)).

This result is in good agreement with those obtained by IR spectroscopy, showing that hydroxyl group, are more stable in xerogel solid. Therefore, the non-calcined xerogel material, presenting the high amount of fluoride removal was selected as adsorbent to continue adsorption procedure in the following experiments.

3.3. Optimization of the adsorption parameters

3.3.1. Effect of adsorbent dose

Adsorption experiments were performed with adsorbent mass varying from 10 to 60 mg. As it appears in Fig. 9, adsorbent dose increasing (up to 20 mg) increases the removal percentage of fluoride due probably to more adsorption sites interacting with F^- anion. Equilibrium fluoride removal was reached when zirconia dose was about 30 mg. This result can be explain by the availability of more excessive active sites at higher adsorbent dose than that is needed for fluoride adsorption with fixed concentration. Therefore, 30 mg was chosen as the optimized adsorption dose. Indeed, the adsorption of fluoride on zirconia can be transferred at the industrial level because it is economic due to the use of a lower adsorbent dose.

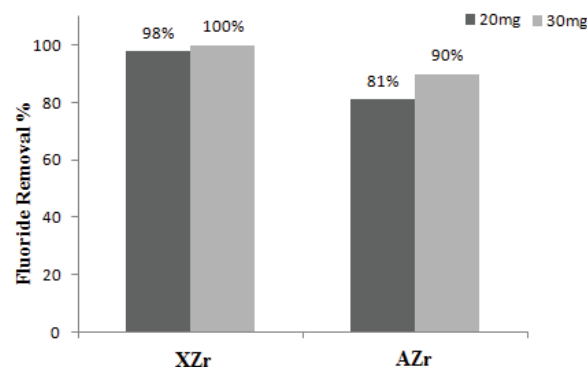


Fig. 8. Effect of drying mode on the fluoride removal ($[F^-] = 5 \text{ mg L}^{-1}$; $\text{pH} = 7$; contact time = 35 min; temperature ($T = 25^\circ\text{C}$)).

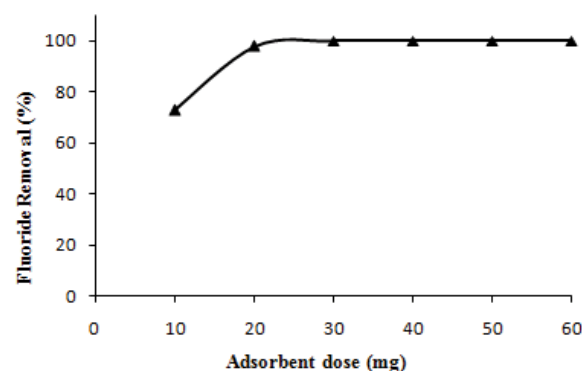


Fig. 9. Effect of adsorbent dose on the fluoride removal ($[F^-] = 5 \text{ mg L}^{-1}$; $\text{pH} = 7$; contact time = 35 min; temperature ($T = 25^\circ\text{C}$)).

3.3.2. Effect of pH

pH solution was an important parameters in adsorption studies. The effect of pH on fluoride adsorption was carried out in a pH range between 2 to 11. As shown in Fig. 10, the high percentage of fluoride removal was observed in acid and neutral medium. However, it decreases in basic medium (pH range from 8 to 10). At lower pH, below to adsorbent pH of zero point charge (pH_{PZC}) ($\text{pH} < \text{pH}_{\text{PZC}} = 7.3$ (Fig. 11)), active site of zirconia was protonated and positive charge at the adsorbent surface exert strong attractive force on anion fluoride. A similar result was observed by Korde et al. [22]. The decrease of fluoride uptake at alkaline pH can be explained by electrostatic repulsion between fluoride anion and negative surface charge of zirconia since at $\text{pH} > \text{pH}_{\text{PZC}}$ the zirconia surface developed negative charge.

At $\text{pH} = \text{pH}_{\text{PZC}}$, the percent of fluoride removal is probably effected by ligand exchange between surface hydroxyl groups and fluoride ion [20].

3.3.3. Effect of contact time and initial fluoride concentration

Kinetic study of fluoride elimination was carried out by varying the contact time adsorbent/adsorbate from 0 to

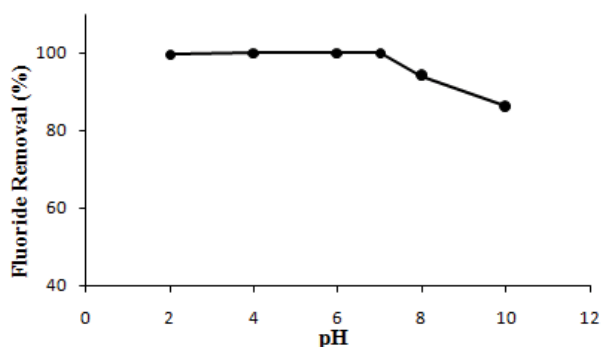


Fig. 10. Effect of pH on the fluoride removal ($[F^-] = 5 \text{ mg L}^{-1}$; adsorbent dose = 30 mg; pH = 7; contact time = 35 min; temperature ($T = 25^\circ\text{C}$)).

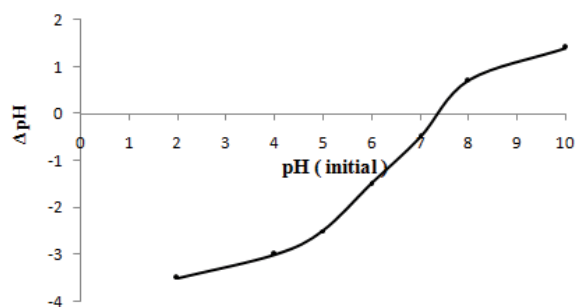


Fig. 11. pH_{PZC} of non-calcined xerogel zirconia.

30 min with an initial adsorbate concentration varying from 2 to 10 mg L^{-1} (Fig. 12).

Results show that fluoride uptake was initially fast (0–5 min) since at the beginning of the adsorption process a high number of active sites were accessible, which remains practically constant as time progresses (from 5 to 25 min), indicating the attainment of adsorption equilibrium; saturation was reached at 25 min. Therefore, the contact time of 25 min was chosen as the optimized. Furthermore, the adsorption process is not affected by the initial concentration of fluoride ions, which could be an advantage.

3.3.4. Regeneration

To investigate reusability of the sorbent, regeneration experiment was conducted (Fig. 13). Results show that the adsorption capacity in Cycles 2 and 3 can reach up 91.9% and 84.8% of that obtained from Cycle 1 respectively. This finding suggests that the sorbent is effective for fluoride removal in multiple cycles.

3.4. Removal fluoride from real sample by xerogel zirconia

In order to verify the effectiveness of fluoride adsorption in natural waters loaded with fluoride by xerogel zirconia. A sample of drinking water from Gafsa City, located in the south of Tunisia was treated with 30 mg of ZrO_2 adsorbent dose at pH 7 within 25 min.

Physico-chemical analysis of this drinking water sample (Table 4) show a complexity of many substances and

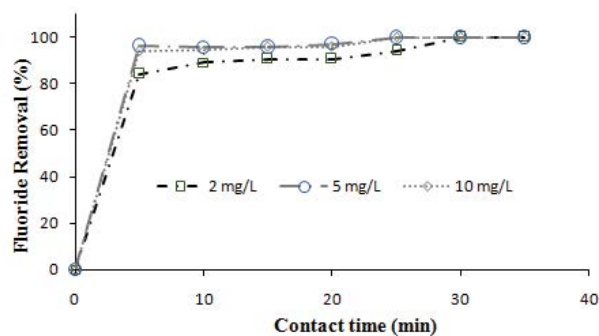


Fig. 12. Effect of contact time on the fluoride removal ($[F^-] = 5 \text{ mg L}^{-1}$; adsorbent dose = 30 mg; pH = 7; contact time = 35 min; temperature ($T = 25^\circ\text{C}$)).

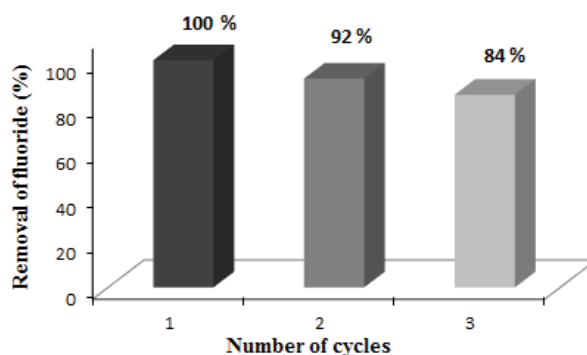


Fig. 13. Efficiency of regenerated XZr material removal (adsorbent dose = 30 mg; pH = 7; contact time = 25 min; temperature ($T = 25^\circ\text{C}$)).

a high fluoride concentration (3.83 mg L^{-1}) exceeding the limit recommended by the WHO (1.5 mg L^{-1}) and Tunisian Potability Standards (NT 09.14) (0.8 mg L^{-1}). After treatment by xerogel zirconia (Table 5), fluoride concentration was reduced from 3.83 to 0.34 mg L^{-1} which confirms the effectiveness of XZr as adsorbent to remove fluoride from aqueous solution below the standards, even in complex matrix.

3.5. Possible adsorption mechanism of fluoride onto xerogel zirconia

To understand the fluoride adsorption mechanism, FTIR analysis was performed on the selected xerogel zirconia adsorbent. The results of FTIR analyses for XZ before and after fluoride adsorption are shown in Fig. 14. It could be seen that after fluoride adsorption the peak of hydroxyl group was shifted from 3468 to 3494 cm^{-1} indicating the participation of the surface hydroxyl groups. In addition, bands at 1629 ($-\text{OH}$ group) and at 1388 cm^{-1} (Zr-OH group) decreases in intensity after fluoride adsorption due to F^- exchange with $-\text{OH}$ and $-\text{O}$ groups [29]. This result demonstrates that fluoride has replaced a substantial fraction of surface hydroxyl groups unbound and bound to zirconium. Indeed, we note a new band at 1552 cm^{-1} characteristics of $[\text{HF}_2]^-$ group [29], which indicated the presence of F^- on the surface of xerogel ZrO_2 . Moreover, bands at 513 , and 740 cm^{-1} characteristic of

Table 4
Characteristics of the natural water samples from Gafsa City in the south of Tunisia

Ion content (mg L ⁻¹)	Water sample
Mg ²⁺	189.6
F ⁻	3.83
SO ₄ ²⁻	1,182
Cl ⁻	420
HCO ₃ ⁻	189
NO ₃ ⁻	18.39
Na ⁺	337
Ca ²⁺	232

Table 5
Comparison of fluoride adsorption of aerogel and xerogel for natural water

	Water sample	Tunisian potability standards (NT 09.14)	WHO standards
[F ⁻] _{initial} (mg L ⁻¹)	3.83		
[F ⁻] _{residual} (mg L ⁻¹)	0.33	0.8	1.5

ZrO₂ increases in intensity after fluoride adsorption probably due to the interaction of fluoride with Zr [22]. This result could be probably due to the formation of fluoride complexes with Zr [32]. Gao et al. [29] confirmed, by FTIR spectroscopy, the presence of new bands at 739.17 and 505.08 cm⁻¹ attributed respectively to Zr-F and [ZrF₅]⁻ groups after fluoride removal by using micron zirconia/zeolite adsorbent.

The scanning electron microscopy (SEM) (Fig. 15a) shows that the surface of XZr is heterogeneous in nature with irregular shapes and many cavities with diameter of 10 μm. On the other hand, SEM of fluoride adsorbed solid XZr-F (Fig. 15b) shows fluoride deposition on the material surface.

Study TEM analysis of XZr indicated the formation of polydispersed Zr nanoparticles (Fig. 15c).

EDS analysis using shows peaks of Zr and O in xerogel zirconia adsorbent (Fig. 16d). After fluoride adsorption

Table 6
Kinetics parameters for fluoride adsorption on xerogel zirconia adsorbent

Equations	First-order kinetics					Second-order kinetics		
	q_{exp} (mg g ⁻¹)	$q_{e,cal}$ (mg g ⁻¹)	k_1	R^2	$q_{e,cal}$ (mg g ⁻¹)	k_2	R^2	

Notes: q_e is the amount of fluoride adsorbed at equilibrium (mg g⁻¹); q_t is the quantity of fluoride adsorbed at the instant 't' (mg g⁻¹), k_1 is the adsorption rate constant for pseudo-first-order reaction (s⁻¹); t is the contact time (s), k_2 is adsorption rate constant for the second-order reaction in (L mg⁻¹ s⁻¹); $q_{e,cal}$ is the adsorption capacity calculated on the basis of the pseudo-first-order and pseudo-second-order equations.

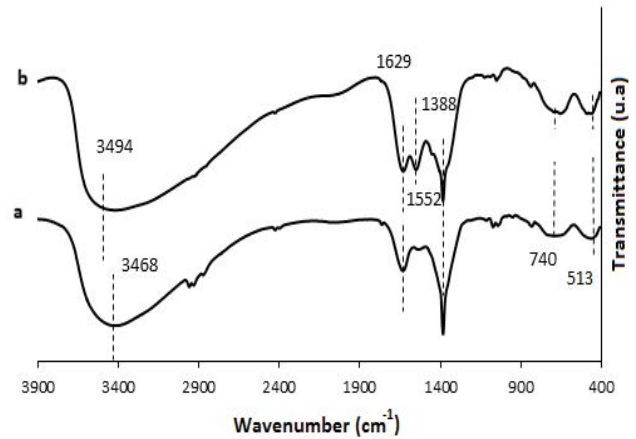


Fig. 14. IR spectra of xerogel before and after fluoride removal: (a) XZ (before fluoride removal) and (b) XZ-F (after fluoride removal).

(Fig. 15e) peak of fluoride appeared indicating adsorption of fluoride on xerogel ZrO₂ surface. In another hand, as it appears in Fig. 16, BET isotherms of fluoride adsorbed xerogel still of type IV with the same hysteresis loop H3. However, we note a change in pores diameter of xerogel zirconia, after fluoride removal, which indicated the insertion of F⁻ into the pore of adsorbent. In addition, the decrease of surface area of XZr-F (Table 2) of about 45% confirmed the saturation of ZrO₂ xerogel adsorbent pores by inserted F⁻.

Finally, all these results show that hydroxyl groups and Zr⁴⁺ sites played an important role in fluoride adsorption process.

3.6. Adsorption kinetics

To predict the mechanism of fluoride adsorption by xerogel zirconia adsorbent, two kinetic models were applied: the pseudo-first-order and the pseudo-second-order [37].

According to these results (Table 6, Fig. 17), it can be concluded that the adsorption experiments follows pseudo-second-order kinetics model ($R^2 \sim 1$). In addition,

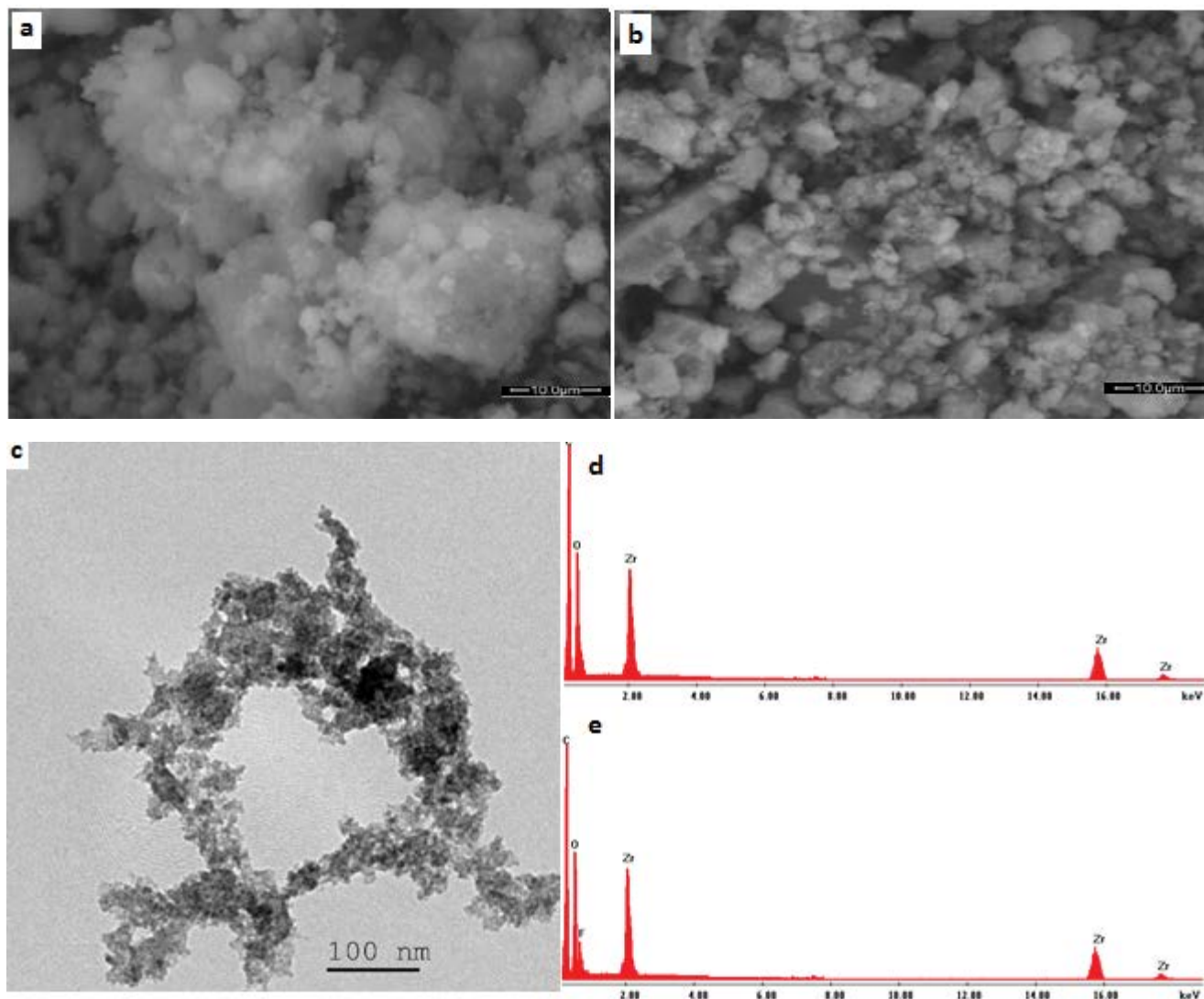


Fig. 15. SEM images of (a) XZr (before fluoride removal), (b) XZr-F (after fluoride removal), TEM image of XZr adsorbent (c) and EDS of (d) XZr (before fluoride removal) and (e) XZr-F (after fluoride removal).

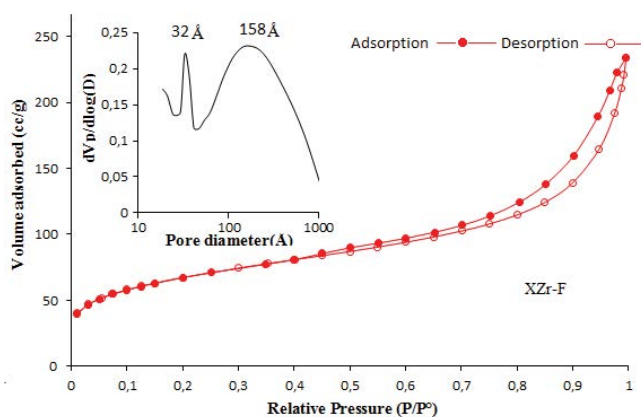


Fig. 16. Adsorption–desorption isotherm and BJH pore distribution of xerogel adsorbent XZr-F after fluoride removal.

equilibrium adsorption capacities (q_e) at the two scales experimental (6.5, 3.27, and 1.55 mg g^{-1}) and theoretical (6.54, 3.25, 1.53 mg g^{-1}) are roughly equal, when the initial fluoride concentrations were 10, 5, and 2 mg L^{-1} , respectively. The adsorption capacity of the xerogel zirconia adsorbent was 6.5 mg g^{-1} for initial fluoride concentration (10 mg L^{-1}), which was higher than other adsorbents reported previously (Table 7).

3.7. Adsorption isotherms

Adsorption isotherm experiment was conducted by using Langmuir and Freundlich isotherms [38,39]. It can be seen from Fig. 18 and Table 8, that the Freundlich adsorption isotherm model ($R^2 = 0.994$) can better describe the behavior of xerogel zirconia adsorption of fluoride, which indicated the adsorption process was a multi-layer adsorption.

4. Conclusion

Xerogel and aerogel zirconia ZrO₂ were successfully prepared using a sol-gel method in one-step with a large specific surface area. Comparative study of textural and structural properties of prepared adsorbents shows that solvent evacuation method and heat treatment play an

important role in hydroxyl group’s stability, which play a key role in fluoride removal process. Xerogel zirconia XZ presents a fluoride adsorption capacity higher than aerogel zirconia AZ adsorbent due to the presence of various types of pores in xerogel solid, which increases the diffusion efficiency and promotes the adsorption performance of fluoride. Also, IR spectroscopy shows that hydroxyl group is more stable in xerogel solid. Zirconia calcination at different temperature decreases the defluorination capacity of the materials related to the loss of surface hydroxyl group, during the heat treatment. The selected xerogel zirconia presents excellent fluoride removal ability from real contaminated natural waters. Kinetic study and adsorption isotherm show that experimental data’s concord very well with the pseudo-second-order and Freundlich model suggested a physisorption process with multilayer adsorption respectively.

Table 7
Comparison of adsorption capacity with different reported adsorbents

Adsorbents	Capacity (mg g ⁻¹)	References
Zr-Mn composite	3.05	[33]
Zirconium impregnated carbon	1.83	[34]
ZrO ₂ -Ze	0.34	[29]
Zr impregnated cellulose	4.95	[35]
Graphene oxide alumina nanocomposite	4.68	[36]
Xerogel zirconia	6.5	This work

Acknowledgment

This work was supported by the Research Supporting Project (RSP- 2021/75), King Saud University (Riyadh, Saudi Arabia).

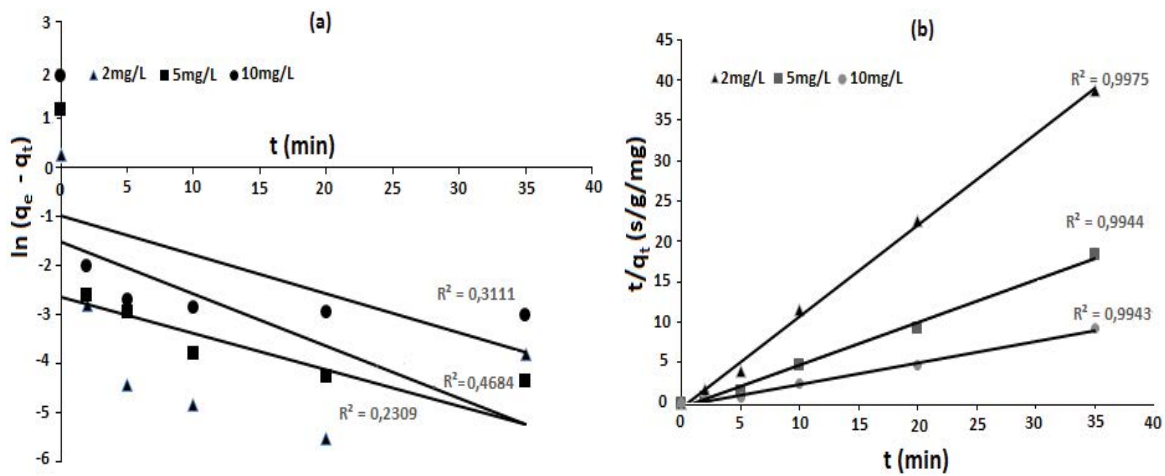


Fig. 17. (a) Pseudo-first-order and (b) pseudo-second-order kinetics.

Table 8
Langmuir and Freundlich adsorption isotherm parameters fluoride adsorption on xerogel zirconia adsorbent

Equations	Langmuir model			Freundlich model		
	K_L (L mg ⁻¹)	q_m (mg g ⁻¹)	R^2	n	K_F	R^2
Equations	$\frac{C_e}{q_e} = \frac{1}{K_L \times q_m} + \frac{C_e}{q_m}$			$\ln q_e = \left(\frac{1}{n}\right) \ln C_e + \ln K_F$		
Parameters	K_L (L mg ⁻¹)	q_m (mg g ⁻¹)	R^2	n	K_F	R^2
Values	3.063	15.748	0.877	1.797	12.716	0.994

Notes: C_e is the equilibrium concentration of fluoride (mg L⁻¹); q_e is the amount of fluoride adsorbed at equilibrium (mg g⁻¹); q_m represents the maximum adsorption capacity of fluoride on per weight of adsorbent (mg g⁻¹); K_L is the Langmuir constant related to the energy of adsorption (L mg⁻¹); K_F is the Freundlich constant related to the relative adsorption capacity of the adsorbent (mg g⁻¹); $1/n$ is the adsorption intensity.

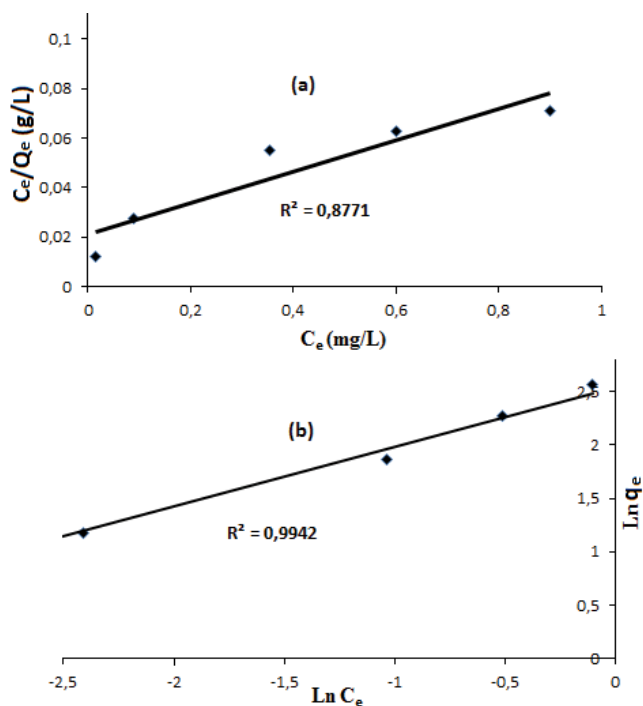


Fig. 18. Adsorption isotherms for fluoride adsorption (a) Langmuir and (b) Freundlich.

References

- S. Karmakar, S. Bhattacharjee, S. De, Aluminium fumarate metal organic framework incorporated polyacrylonitrile hollow fiber membranes: spinning, characterization and application in fluoride removal from groundwater, *Chem. Eng. J.*, 334 (2018) 41–53.
- W. Guissouma, J. Tarhouni, Fluoride in Tunisian drinking tap water, *J. Water Resour. Prot.*, 7 (2015) 860–870.
- D.L. Ozsvath, Fluoride and environmental health: a review, *Rev. Environ. Sci. Biotechnol.*, 8 (2009) 59–79.
- WHO, International Standards for Drinking Water, World Health Organization, Geneva, 2009.
- S.I. Bouhadjar, H. Kopp, P. Britsch, S.A. Deowan, J. Hoinkis, J. Bundschuh, Solar powered nanofiltration for drinking water production from fluoride-containing groundwater – a pilot study towards developing a sustainable and low-cost treatment plant, *J. Environ. Manage.*, 231 (2019) 1263–1269.
- J. Chen, H. Qian, H. Wu, Y. Gao, X. Li, Assessment of arsenic and fluoride pollution in groundwater in Dawukou area, Northwest China, and the associated health risk for inhabitants, *Environ. Earth Sci.*, 76 (2017) 314, doi: 10.1007/s12665-017-6629-2.
- T.J. Robshaw, R. Dawson, K. Bonser, M.D. Ogden, Towards the implementation of an ion-exchange system for recovery of fluoride commodity chemicals. Kinetic and dynamic studies, *Chem. Eng. J.*, 367 (2019) 149–159.
- K.K. Yadav, N. Gupta, V. Kumar, S.A. Khan, A. Kumar, A review of emerging adsorbents and current demand for defluoridation of water: bright future in water sustainability, *Environ. Int.*, 111 (2018) 80–108.
- A. Teutli-Sequeira, V. Martínez-Miranda, M. Solache-Ríos, I. Linares-Hernández, Aluminium and lanthanum effects in natural materials on the adsorption of fluoride ions, *J. Fluorine Chem.*, 148 (2013) 6–13.
- A. Goswami, M.K. Purkait, The defluoridation of water by acidic alumina, *Chem. Eng. Res. Des.*, 90 (2012) 2316–2324.
- S.M. Prabhu, S. Meenakshi, Synthesis of metal ion loaded silica gel/chitosan biocomposite and its fluoride uptake studies from water, *J. Water Process Eng.*, 3 (2014) 144–150.
- T. Wajima, Y. Umetsu, S. Narita, K. Sugawara, Adsorption behavior of fluoride ions using a titanium hydroxide-derived adsorbent, *Desalination*, 249 (2009) 323–330.
- P. Sengupta, S. Saha, S. Banerjee, A. Dey, P. Sarkar, Removal of fluoride ion from drinking water by a new $\text{Fe}(\text{OH})_3/\text{nano CaO}$ impregnated chitosan composite adsorbent, *Polym. Plast. Technol. Mater.*, 59 (2020) 1191–1203.
- N. Kamoun, M.K. Younes, A. Ghorbel, A.S. Mamède, A. Rives, Effect the solvent evacuation mode on the catalytic properties of nickel-modified sulfated zirconia catalysts: *n*-hexane isomerization, *React. Kinet. Mech. Catal.*, 111 (2014) 199–213.
- Y.Y. Sun, S.Q. Ma, Y.C. Du, L. Yuan, S.C. Wang, J. Yang, F. Deng, F.-S. Xiao, Solvent-free preparation of nanosized sulfated zirconia with Brønsted acidic sites from a simple calcination, *J. Phys. Chem. B*, 109 (2005) 2567–2572.
- S. Marullo, C. Rizzo, N.T. Dintcheva, F. Giannici, F. D’Anna, Ionic liquids gels: soft materials for environmental remediation, *J. Colloid Interface Sci.*, 517 (2018) 182–193.
- M.K. Mishra, B. Tyagi, R.V. Jasra, Synthesis and characterization of nano-crystalline sulfated zirconia by sol-gel method, *J. Mol. Catal. A: Chem.*, 223 (2004) 61–65.
- F. Schmidt, New catalyst preparation technologies—observed from an industrial viewpoint, *Appl. Catal., A*, 221 (2001) 15–21.
- X. Dou, D. Mohan, C.U. Pittman Jr., S. Yang, Remediating fluoride from water using hydrous zirconium oxide, *Chem. Eng. J.*, 198 (2012) 236–245.
- S.B. Patel, A.K. Panda, S.K. Swain, T. Patnaik, F. Muller, S. Delpeux-Ouldriane, L. Duclaux, R.K. Dey, Development of aluminum and zirconium based xerogel for defluoridation of drinking water: study of material properties, solution kinetics and thermodynamics, *J. Environ. Chem. Eng.*, 6 (2018) 6231–6242.
- IUPAC Recommendations, *Pure Appl. Chem.*, 66 (1994) 1739.
- S. Korde, S. Tandekar, R.M. Jugade, Novel mesoporous chitosan-zirconia-ferrosoferric oxide as magnetic composite for defluoridation of water, *J. Environ. Chem. Eng.*, 8 (2020) 104360, doi: 10.1016/j.jece.2020.104360.
- J. Wang, W.H. Xu, L. Chen, Y. Jia, L. Wang, X.-J. Huang, J.H. Liu, Excellent fluoride removal performance by $\text{CeO}_2\text{-ZrO}_2$ nanocages in water environment, *Chem. Eng. J.*, 231 (2013) 198–205.
- C.-F. Chang, C.-Y. Chang, T.-L. Hsu, Removal of fluoride from aqueous solution with the superparamagnetic zirconia material, *Desalination*, 279 (2011) 375–382.
- Z.C. Yu, C.H. Xu, K.K. Yuan, X.Z. Gan, C. Feng, X.Q. Wang, L.Y. Zhu, G.H. Zhang, D. Xu, Characterization and adsorption mechanism of ZrO_2 mesoporous fibers for health-hazardous fluoride removal, *J. Hazard. Mater.*, 346 (2018) 82–92.
- J.S. He, J. Paul Chen, A zirconium-based nanoparticle: essential factors for sustainable application in treatment of fluoride containing water, *J. Colloid Interface Sci.*, 416 (2014) 227–234.
- X.M. Dou, D. Mohan, C.U. Pittman Jr., S. Yang, Remediating fluoride from water using hydrous zirconium oxide, *Chem. Eng. J.*, 198–199 (2012) 236–245.
- N. Kamoun, M.K. Younes, A. Ghorbel, A.S. Mamède, A. Rives, Comparative study of the texture and structure of aerogel and xerogel sulphated zirconia doped with nickel, *J. Porous Mater.*, 19 (2012) 375–381.
- Y. Gao, M.F. Li, Y.F. Ru, J.X. Fu, Fluoride removal from water by using micron zirconia/zeolite molecular sieve: characterization and mechanism, *Groundwater Sustainable Dev.*, 13 (2021) 100567, doi: 10.1016/j.gsd.2021.100567.
- X.M. Wu, Y. Zhang, X.M. Dou, M. Yang, Fluoride removal performance of a novel Fe–Al–Ce trimetal oxide adsorbent, *Chemosphere*, 69 (2007) 1758–1764.
- J. Wang, D.J. Kang, X.L. Yu, M.F. Ge, Y.T. Chen, Synthesis and characterization of Mg–Fe–La trimetal composite as an adsorbent for fluoride removal, *Chem. Eng. J.*, 264 (2015) 506–513.
- X.M. Dou, D. Mohan, C.U. Pittman Jr., S. Yang, Remediating fluoride from water using hydrous zirconium oxide, *Chem. Eng. J.*, 198 (2012) 236–245.

- [33] V. Tomar, S. Prasad, D. Kumar, Adsorptive removal of fluoride from water samples using Zr–Mn composite material, *Microchem. J.*, 111 (2013) 116–124.
- [34] G. Alagumuthu, M. Rajan, Equilibrium and kinetics of adsorption of fluoride onto zirconium impregnated cashew nut shell carbon, *Chem. Eng. J.*, 158 (2010) 451–457.
- [35] M. Barathi, A.S.K. Kumar, N. Rajesh, A novel ultrasonication method in the preparation of zirconium impregnated cellulose for effective fluoride adsorption, *Ultrason. Sonochem.*, 21 (2014) 1090–1099.
- [36] N. Xu, S. Li, W. Li, Z. Liu, Removal of fluoride by graphene oxide/alumina nanocomposite: adsorbent preparation, characterization, adsorption performance and mechanisms, *ChemistrySelect*, 5 (2020) 1818–1828.
- [37] D. David, R. Caplain, *Méthodes usuelles de caractérisation des surfaces*, Eyrolles, Paris, 1988, 374 p.
- [38] I. Langmuir, The adsorption of gases on plane surfaces of glass, mica and platinum, *J. Am. Chem. Soc.*, 40 (1918) 1361–1403.
- [39] H.M.F. Freundlich, Über die Adsorption in Lösungen, *Z. Phys. Chem.*, 57 (1906) 385–470.